Carbon Market Risk Estimation Using Quantum Generative Adversarial Network and Amplitude Estimation

Xiyuan Zhou, Huan Zhao, Yuji Cao, Xiang Fei, Gaoqi Liang and Junhua Zhao

***Abstract*—Accurately and efficiently estimating carbon market risk is paramount for ensuring financial stability, promoting environmental sustainability, and facilitating informed decision-making. Although classical risk estimation methods are extensively utilized, the implicit pre-assumptions about distribution are predominantly contained and challenging to balance accuracy and computational efficiency. A quantum computing-based carbon market risk estimation framework is proposed to address this issue with the quantum conditional generative adversarial networks-quantum amplitude estimation (QCGAN-QAE) algorithm. Specifically, QCGAN is employed to simulate the future distribution of the generated loss rate, whereas QAE is applied to measure the distribution. Also, the quantum circuit of the QCGAN improved by reordering the data entanglement layer and data rotation layer, coupled with the introduction of the quantum fully connected layer. And the binary search method is incorporated into the QAE to bolster the computational efficiency. The simulation results based on the European Union Emissions Trading System manifest that the proposed framework markedly enhances the efficiency and precision of Value-at-Risk (VaR) and Conditional Value-at-Risk (CVaR) compared to original methods.**

***Index Terms*—Quantum generative adversarial networks, quantum amplitude estimation, carbon market, risk estimation.**

I. INTRODUCTION

THE international society commits to a consensus on carbon emission reduction in response to the severe challenges of rising global temperatures and environmental degradation [1]. To realize this collective vision, the establishment of carbon markets has been recognized as an essential and flexible strategy. Among the carbon markets of various countries and regions, the European Union Emissions Trading System (EU ETS) is pivotal in mitigating greenhouse gas emissions through market mechanisms [2]. However, the EU carbon market is frequently challenged by price volatility due to factors such as supply-demand dynamics, policy adaptations, and global economic condition changes, consequently amplifying the financial risks inherent to the carbon market. Imprecise risk estimates may result in significant financial losses for the market participants. Thus, it becomes imperative to employ refined techniques to estimate carbon market risks accurately.

To enhance the accuracy of market risk estimation, existing research has explored three main methods: time series model, capital asset pricing model and Monte Carlo simulation. Each method corresponded to a different risk measure. For time series models, when applied to historical data, it can compute the volatility and variance of financial assets, offering investors an initial measure of market price or return fluctuations [3][4]. The capital asset pricing model determines the Beta coefficient [5][6]. This coefficient measures an asset's systemic risk, indicating its sensitivity relative to the overall market [7][8]. The Monte Carlo simulation, simulating a myriad of potential price paths, forecasts the future distribution of assets, providing investors with crucial risk measures such as Value-at-Risk (VaR) and Conditional Value-at-Risk (CVaR) [9][10]. VaR and CVaR emphasize potential losses in extreme scenarios, capable of capturing the nonlinear and asymmetrical risks, and are more precisely to reflect the risk level of the carbon market [11][12]. However, traditional methods for estimating VaR and CVaR, such as the Monte Carlo simulation, require many simulations to achieve a reliable estimate and often operate on implicit assumptions of data probability distributions, which may only sometimes reflect reality [13]. In light of these challenges, the exploration of quantum algorithms emerges as a promising frontier, promising a more efficient and precise avenue for risk estimation.

Existing quantum computing research on risk estimation primarily revolves around the simulation process and utilizes quantum amplitude estimation (QAE) to improve computational efficiency and accuracy [14][15]. However, most studies simulate distributions using pre-assumed models to generate data, such as the Gaussian conditionally independent model [16][17]. Such assumptions may not align with the market dynamics and could cause biases. Conditional Generative Adversarial Network is widely used to model data distributions and its quantum version, Quantum Conditional Generative Adversarial Network (QCGAN), is regarded as a technology that also has great potential in data distribution simulation in real-world applications, such as image generation [18][19][20]. Combining QAE, QCGAN, and binary search, our research pioneers the application of quantum computing in carbon market risk estimation. The integration of QCGAN significantly improves the efficiency and accuracy, while utilizing binary search solves the problem of QAE's inefficiency in searching for VaR, thereby improving the efficiency of the entire risk estimation. Together, these improvements represent a significant advancement in risk estimation.

To solve the above-mentioned issues, a quantum computing-based framework is proposed to estimate the risk in the carbon market. The contributions of this article are summarized as follows.

1) A QCGAN-QAE framework is proposed for carbon market risk estimation, which innovatively combines QCGAN and QAE to enhance the accuracy and efficiency of market risk estimation. To the best of our knowledge, we are among the first to apply quantum computing in carbon market risk estimation.
2) The circuit structure of the quantum generator in QCGAN is improved by reordering the data entanglement layer and data rotation layer, coupled with the introduction of the quantum fully connected layer before rotation operations.
3) To improve the computational efficiency, the binary search approach is incorporated with QAE, rooted in quantum coding, which adeptly delineates the spatial boundaries for the good states in QAE.

The remaining sections are organized as follows. Section II introduces related work on QCGAN and QAE. The proposed QCGAN-QAE framework for carbon market risk estimation and the modified QCGAN and QAE methods are illustrated in Section III. Section IV shows the experiment results of the proposed methods with the EU ETS data. The conclusion and discussion are provided in the last section.

II. Background

Machine learning algorithms are widely used in the energy field [21][22]. Quantum computing leverages the principles of quantum mechanics to process information in fundamentally different ways from classical computers [23]. For the carbon market risk estimation problems, QCGAN generates the risk distribution. QAE is used to efficiently measure the distribution, obtaining the risk estimation indicators VaR and CVaR [24].

A. Quantum Conditional Generative Adversarial Network

CGANs incorporate conditional data to boost generation accuracy [25][26]. Quantum properties, specifically superposition and entanglement, improve the performance of generative modeling [20]. The key components of QCGAN include a generator, discriminator, and objective function.

1) Generator

The generator in QCGAN is constructed as a Parameterized Quantum Circuit (PQC), which is a quantum circuit with adjustable parameters and can be optimized during training. The PQC encodes conditional constraints as an input quantum state $|\psi(y)\rangle$ and outputs a quantum state $|\psi_{out}\rangle$ as the generated data sample. For a specified condition state $|\psi(y)\rangle$ and an initialized random state $|\psi(z)\rangle$, the quantum transformation governed by the PQC is given by:

$$|\psi_{out}\rangle = U(\theta)(|\psi(y)\rangle \otimes |\psi(z)\rangle) \quad (1)$$

where $U(\theta)$ denotes the PQC with parameters θ, and $\otimes$ is the tensor product.

2) Discriminator

The discriminator D in QCGAN integrates a classical neural network to classify quantum states into real or generated data samples. For an input data χ, D yields a probability p indicating the authenticity of χ, to represent whether it is genuine or generated by the generator. This is formally expressed as:

$$p_{QCGAN} = D(\chi) \quad (2)$$

The primary training goal for D is to accurately classify the quantum states.

3) Objective Function

The key of CGAN is adversarial training, which minimizes the quantum Jensen-Shannon divergence. During training, the discriminator D tries to maximize the differentiation of real data from the output of the generator $G(z|y)$. At the same time, the generator G aims to generate data that the discriminator considers to be real, i.e., to minimize the difference between the generated data and the real data. The optimization of QCGAN can be formulated as a min-max problem:

$$\min_G \max_D \left(E[\log D\,(x|y)] + E\left[\log\left(1 - D(G(z|y))\right)\right]\right) \quad (3)$$

where $E[.]$ represents mathematical expectation.

B. Quantum Amplitude Estimation

QAE aims to estimate the amplitude of a particular state within a quantum system [27]. This algorithm can be regarded as a natural extension of Quantum Amplitude Amplification (QAA) [28].

In the quantum mechanics, amplitude directly corresponds to probability. Consider the quantum state [29]:

$$|\psi\rangle = \sqrt{1 - p_{QAE}}|\psi_0\rangle + \sqrt{p_{QAE}}\,|\psi_1\rangle \quad (4)$$

where $|\psi_0\rangle$ and $|\psi_1\rangle$ are normalized states, and p_{QAE} is a real number. The goal of QAE is to estimate the amplitude a and the square of the amplitude a is equivalent to the probability, i.e., $|a|^2 = p_{QAE}$. Within the QAE framework, the angle θ is used to represent the amplitude a, with $a = \sin\theta$, leading to $\sin^2\theta = p_{QAE}$. Such a transformation provides an avenue for the use of rotation operations to modulate the amplitude. The formula after substitution is as follows:

$$|\psi\rangle = cos\theta\,|\psi_0\rangle + \sin\theta|\psi_1\rangle \quad (5)$$

Based on the above analysis, the measurement of probability is converted into the measurement of angle θ, and the core is to amplify θ. In order to amplify θ, the key is to have an $\mathcal{A}$ that can be used repeatedly and an oracle $\widehat{\chi_{\varphi_0}}$ that can identify the marked state $\widehat{\chi_0}$. So consider a specific operator:

$$\widehat{\chi_\varphi} = I - 2\,|\varphi\rangle\langle\varphi| \quad (6)$$

This operator assigns a sign flip to the state $|\varphi\rangle$. Given an oracle $\widehat{\chi_{\varphi_0}}$ that interacts specifically with the marked state $|\psi_0\rangle$, and with the ability to repeatedly apply $\mathcal{A}$ and $\mathcal{A}^\dagger$, the operation $\mathcal{A}\widehat{\chi_0}\mathcal{A}^\dagger = I - 2\,|\psi\rangle\langle\psi|$ can be executed on the encoded state $|\psi\rangle$. Then the "Grover" operator Q is defined as [27]:

$$Q = \mathcal{A}\widehat{\chi_0}\mathcal{A}^\dagger\widehat{\chi_{\varphi_0}} \quad (7)$$

This operator ensures that the system, after a certain number of Grover iterations, reaches the state:

$$\psi_E(k) = Q^k|\psi\rangle = \cos\left((2k+1)\theta\right)|\psi_0\rangle + \sin\left((2k+1)\theta\right)|\psi_1\rangle \quad (8)$$

By appropriately selecting the iteration count k, the amplitude of the target quantum state can be amplified to a

desired level, facilitating accurate amplitude estimation during measurement.

C. Market Risk Evaluation Metrics

VaR and CVaR are commonly used risk metrics in finance to quantify the potential loss in value of a risky portfolio over a given period for a given confidence level. VaR provides an estimate of the maximum potential loss an investment portfolio [30]. The formula of VaR is as follows:

$$P(L > VaR_\alpha) = 1 - \alpha \tag{9}$$

where P represents the probability, L represents the loss over a given period, α represents the confidence level.

CVaR calculates the expected value of the loss since it already exceeds VaR, which makes it better to consider extreme losses [31]. The formula of CVaR is as follows:

$$CVaR_\alpha = \frac{1}{1-\alpha}\int_{L>VaR_\alpha} L\, f(L)\, dL \tag{9}$$

where $f(L)$ is the probability density function of the loss L.

III. Quantum-based Carbon market Risk Estimation Framework

A. Carbon Market Risk Estimation Based on Quantum Algorithm

To effectively address the challenges faced in previous research, including requiring a large number of measurements, consuming computing resources and having implicit assumptions reducing accuracy, the quantum computational framework based on the QCGAN and QAE algorithms is introduced. The synergy of these two algorithms allows us to refine risk estimates for carbon markets. The overall structure of the proposed framework is depicted in Fig. 3, including data preprocessing, risk distribution learning, risk distribution measuring, and risk evaluation. The data preprocessing converts original market data into standardized quantum state data. Then in the risk distribution learning, the QCGAN is trained with the quantum state data to generate the simulated one-day risk distribution. The risk distribution measuring combines QAE with the binary search method to measure the previously obtained risk distribution, find the target quantum state corresponding to VaR, and measure the probability distribution of the quantum state required to calculate CVaR. Finally, VaR and CVaR are calculated with the measured results in the risk evaluation part. The specific details of the framework are as follows:

1) Data Preprocessing

In this stage, the loss rate is calculated and converted into binary quantum encoding to serve as the input, providing the foundation for subsequent quantum computations. We calculate the loss rate $[y_1, \ldots, y_T]$, which is the negative number of the rate of return R, from carbon market price data $[p_0, \ldots, p_T]$, T is the total number of days. The formula is as follows:

$$y_t = -R_t = -\frac{(p_t - p_{t-1})}{p_{t-1}} \tag{10}$$

The historical loss rate in the past N days $[y_{t-N}, \ldots, y_{t-1}]$ is used as conditional data to simulate future data generation for the object. The future loss rate y_t is used as the object data χ_t. Loss rate is chosen to measure risk rather than price because, starting from the definitions of VaR and CVaR, investors tend to pay more attention to the rate of change of price rather than its absolute value. Binary encoding techniques are used to convert these classical data into quantum data. The loss rate is first normalized using the min-max method and evenly divided into 2^n segments according to the numerical value, where n is the number of qubits required for encoding. Next, we convert the numerical value of each segment into a binary format for processing in quantum computing. In addition, to train and evaluate the model, we divide the data set into two key parts: the training set and the test set. The training set is used to train our model to understand and capture the characteristics of the data. The test set is used to evaluate the performance of the model.

2) Risk Distributions Learning

Subsequently, to simulate potential future loss rate distributions, we deploy QCGAN. We provide the quantum generator with the historical loss rate previously transformed into quantum states as conditional data. A special feature of QCGAN is the incorporation of conditional data $|y\rangle$ and noise $|z\rangle$. Among them, y is the previously preprocessed quantum data of the past n days, i.e., $[y_n, y_{n-1}, \ldots, y_{t-1}]$; z is the quantum noise. This noise offers an element of randomness to the generator and serves as supplementary information, assisting the generator in producing samples with distinct characteristics. Consequently, the generator combines these conditional data with noise, producing samples that represent potential future loss rate distributions. The samples generated by the generator are subsequently passed to the classical discriminator. The most important function of the discriminator is to differentiate between the samples created by the generator and actual data samples, providing an evaluation score in the process. Upon receiving feedback from the classical discriminator, both the quantum generator and the discriminator optimize their parameters using the backpropagation algorithm. With each iteration, there is a progressive optimization of both the generator and discriminator parameters. Once a predetermined number of iterations are reached or a specific accuracy threshold is met, when the generator simulates future loss rate distributions with extremely high accuracy.

3) Risk Distribution Measuring

To improve the efficiency of measuring the predicted quantum state generated by the quantum generator, obtain the target quantum state corresponding to VaR and the quantum state and its probability required to calculate CVaR, we used QAE combined with binary search. The process starts with a binary search, which divides the quantum state into two subspaces based on the median value of all quantum states, i.e., $|10\ldots0\rangle$. The set of quantum states composed of quantum states greater than or equal to the median is measured, i.e., $|1x\ldots x\rangle$. Then we use QAE to measure the probability sum of the quantum state set's quantum states. The next step is to confirm the target quantum state. Specifically, the probability sum of measured quantum states is compared with 1-α, where α is the

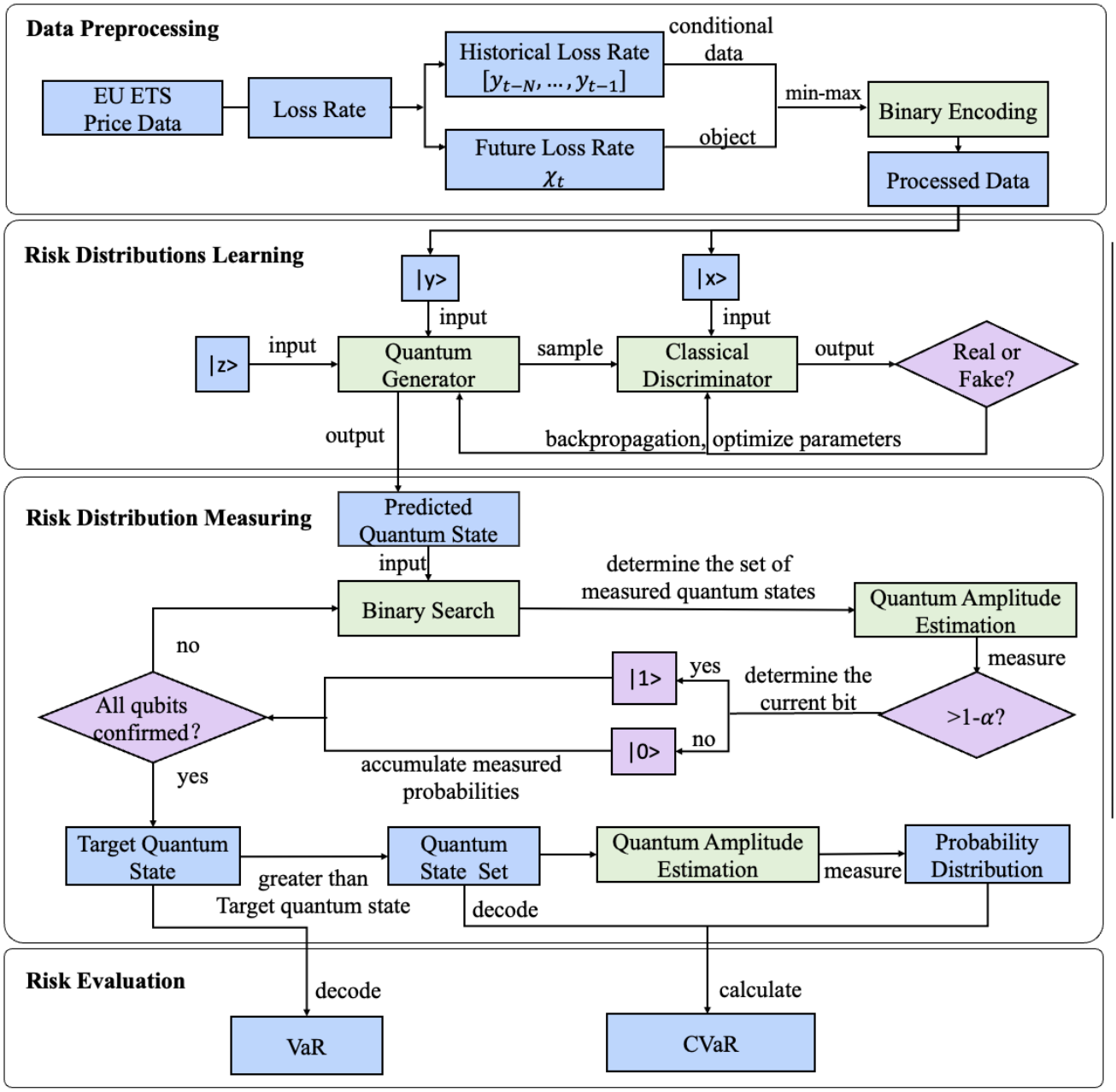

Fig. 1. Carbon market risk estimation based on QCGAN-QAE framework.

confidence level. If the probability sum is greater than 1-α, which means that the target quantum state is larger than the median, then we determine the current qubit to be $|1\rangle$; otherwise, the target quantum state is smaller than the median, the current qubit is $|0\rangle$, and accumulate the probability sum of measured quantum states. In this way we confirm the current qubit of the target quantum state. Then go back to the binary search to search for the more precise target quantum state and determine the next qubit until all qubits are determined, and finally get the whole target quantum state, which is the quantum state corresponding to VaR. After determining the target quantum state, all quantum states greater than the target quantum state correspond to extreme loss rates greater than VaR. This set of quantum states is required to calculate CVaR. Use QAE to measure these quantum states and obtain their probability distribution, which provides a data source for subsequent calculations.

4) Risk Evaluation

The final step is risk evaluation. For VaR, initially, the target quantum state is determined through QAE combined with binary search, VaR can be obtained just by decoding the target quantum state. For CVaR, by decoding the quantum states in the quantum state set and the corresponding probabilities, the CVaR is calculated. The specific formula is as follows:

$$CVaR_\alpha = \frac{1}{1-\alpha}\sum_{L>VaR_\alpha} L\, f(L) \qquad (11)$$

where α is the confidence level, L is the loss rate obtained after decoding the quantum state set, $f(L)$ is the corresponding probability.

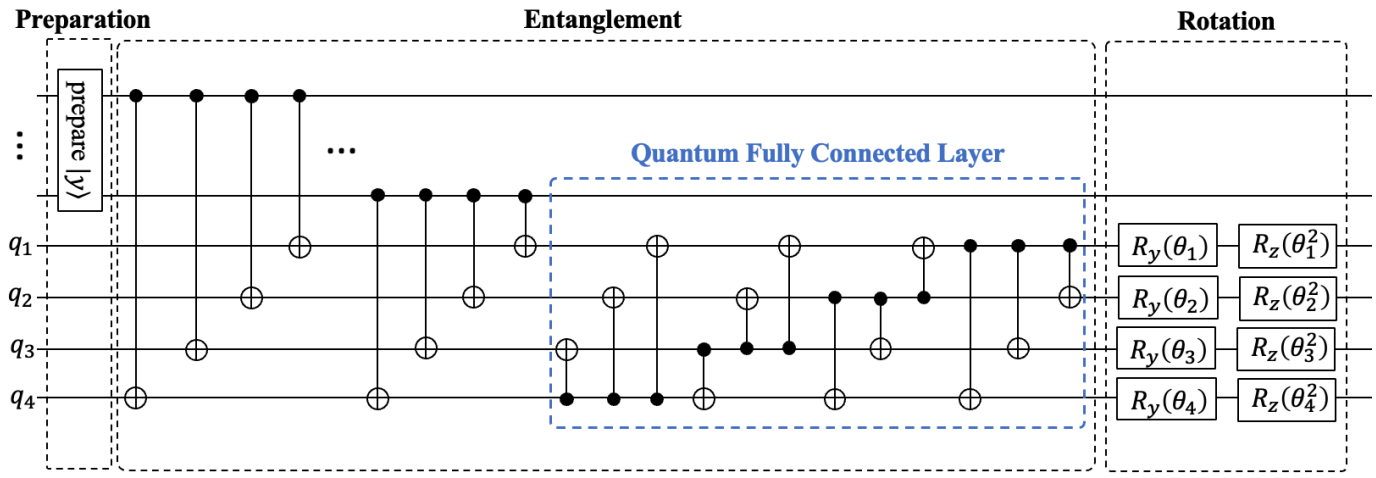

Fig. 2. The quantum circuit of the generator (using the generation of data that requires four qubits as an example).

B. Improved Quantum Conditional Generative Adversarial Network for Generating Simulated Risk Distribution

Accurately simulating the distribution of loss rate is crucial for risk estimation and the QCGAN is employed and improved in this paper. Specifically, the PQC structure of the generator is enhanced. Compared to previous models in quantum-based risk estimation, the improved QCGAN exhibits better performance generating of precise quantum states. The generator, discriminator and learning process of improved QCGAN for risk distribution generating are described as follows.

For the generator, the main part is PQC, aiming to simulate the fundamental dynamics of the loss rate. The PQC includes several parametrized quantum gates, such as rotation gates and controlled-not (CNOT) gates, and the parameters are adjusted through discriminator-based feedback. The proposed circuit incorporates three stages: preparation, entanglement, and rotation (see Fig. 4). The preparation stage encodes the market condition state $|y\rangle$ into quantum states. The entanglement stage ensures that the encoded condition state interacts well with the noise. The rotation stage is responsible for generating risk distribution. The design and operation of these three modules will be introduced later in this section. To enhance the expressive capability of the generator and capture the complex relationships within market data, we introduced a Quantum Fully Connected layer (QFC) in the entanglement stage. The QFC layer comprises a series of CNOT gates and rotation gates to achieve full connectivity among qubits, which can facilitate interactions among all qubits. Such a fully connected structure ensures that no crucial interaction information is lost during the entanglement process, thus enhancing the accuracy of carbon market simulation. The specific circuit structure is depicted in Fig. 4. The details of QFC are introduced later in this section.

For the discriminator, the classic Fully Connected Neural Network is employed to distinguish real data and generated data as the binary classification problem [32]. The inputs of the discriminator are randomly chosen from real data $x|y$ or the quantum generator $G(z|y)$. The output of the discriminator is a scalar in the range of [0,1], representing the probability of the input data being regarded as real data. The neural network comprises multiple convolution layers, each followed by a ReLU activation function, with the final layer utilizing a Sigmoid activation function to map the output to the range (0,1). The dimension of the input layer in the discriminator matches the number of qubits in the quantum generator to facilitate direct interaction between quantum and classical data [33]. The structure of hidden layers can be adjusted based on the complexity of the task.

For the learning process, both the generator and discriminator are co-trained using the Adam algorithm. The discriminator's training frequency is adjusted for stability and binary cross-entropy loss is used for optimization. Throughout the training process, the Jensen-Shannon divergence is used to measure the difference between the distribution of the generated quantum states by the generator and the real data distribution. Based on this measurement, adjustments can be made to refine the generator. When optimizing parameters, the traditional neural network-based discriminator can directly compute the gradient of the loss function through backpropagation. However, in variational quantum circuits, due to their complex quantum properties, we cannot directly calculate the gradient of the loss function like traditional neural networks, so we use the parameter shift rule to estimate the partial derivatives [33], thereby enabling the use of the same quantum circuit to compute gradient information. This collaborative optimization process of generator and discriminator provides the ability of QCGAN to accurately generate loss rate distributions. Through continuous feedback and optimization loops, the generator can produce outputs that are increasingly closer to the actual data distribution, while the discriminator's distinguishing ability also gradually improves, thereby achieving good results in simulating loss rate distributions.

The specific details of our generator modifications are as follows:

1) Swap Entanglement and Rotation

To accurately simulate the quantum state of loss rate distribution, a novel quantum circuit of the generator is proposed. As illustrated in Fig.4, the generator's quantum circuit contains three key stages: the preparation stage, the entanglement stage, and the rotation stage. In earlier research,

the quantum circuit typically proceeded with the rotation stage before the entanglement stage [20]. However, we discovered that placing the entanglement stage before the rotation stage can significantly enhance the efficiency and expressive capability of the quantum circuit. Firstly, through the prior entanglement operation, strong quantum correlations are established before the rotation operation, providing favorable conditions for the subsequent rotation stage. Such strong quantum correlations empower the quantum circuit to better explore and utilize the multi-dimensional characteristics of quantum space during the rotation stage, thus improving the expressive capability of the quantum circuit. Secondly, based on the already entangled quantum states, the rotation operations can adjust the quantum states more accurately and purposefully, possibly reducing the number of required rotation operations, thereby improving the efficiency and accuracy of the quantum circuit. The specific functionalities of each stage will be detailed below.

Initiating with the preparation stage, the main goal of quantum circuits is to encode binary quantum data into the quantum circuit. This is accomplished by passing through the X gate. For example, encoding $|0101\rangle$ applies X gates to the qubits where $|0\rangle$ is located, that is, the first and third qubits. Such operations not only ensure that quantum states start from a representation that is consistent with classical conditions, but also lay the foundation for subsequent quantum interactions.

The subsequent stage is entanglement, which significantly deviates from conventional architectures. Traditionally, the rotation stage precedes the entanglement stage. Our revised model prioritizes establishing a coherent relationship between the condition and noise qubits ahead of rotation. Among them, conditional qubits refer to qubits that encode conditional data, and noise qubits refer to qubits that encode noise. By leveraging CNOT gates, a deterministic link is instituted, where the state of the qubits encoding the conditional data will directly influence the qubits corresponding to the noise. Initiating the interaction before simulation ensures that the quantum states of the noise qubits are predisposed by the condition, thus enhancing the efficiency and accuracy of the subsequent rotation.

The last stage is rotation, that is, qubits undergo a sequence of operations by RY rotation gates and RZ rotation gates [34]. These rotation gates are parameterized by values in θ, allowing continuous adjustment to better simulate the desired quantum data states.

By deploying these rotation and entanglement gates in a structured and orderly manner, the quantum states evolve coherently and can progressively converge to the target configuration.

2) Quantum Fully Connected Layer

The fully connected layer in classical neural networks suggests that each neuron in the previous layer is connected to every neuron in the next layer. Similarly, in the QFC layer, every qubit interacts with every other, facilitating a full exchange of quantum information across the circuit. This interaction is achieved by applying the CNOT gate between every pair of qubits, ensuring that each qubit can influence every other qubit. By enabling interactions among all qubits, the QFC layer ensures that no qubit remains isolated. This leads to a more holistic information flow across the quantum circuit, potentially accelerating convergence during training and achieving a more refined representation of quantum states.

As shown in Fig. 5, taking the four-qubit system as an example, the common connection topologies of qubits include three types: circular, weakly fully connected and strongly fully connected. Previous research has shown that, although the circular topology requires fewer quantum gates, it needs more layers to meet the entanglement requirements of complex tasks [33][35][36]. The fully connected layers currently used in QGAN are weakly fully connected (see Fig. 5(b)), that is, there is only a one-direction connection between all qubits, but this connection is not sufficient and may reduce learning ability [20][37]. Therefore, this paper applies the strongly connected fully connected layer to the entanglement stage [38]. The specific connection method and location of QFC in the generator are shown in Fig.4.

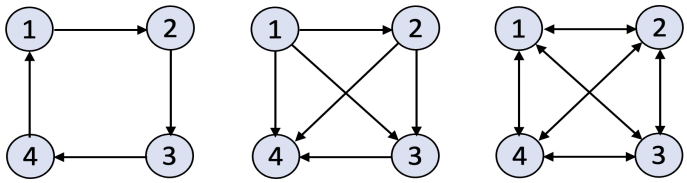

Fig. 3. Three common qubit-to-qubit connection topologies.

C. Quantum Amplitude Estimation Combined with Binary Search for Measuring Risk Distribution

For the quantum-based risk estimation method, to accurately and efficiently estimate the risks associated with the carbon market, we need to measure the quantum states generated by QCGAN. To this end, QAE is employed. In contrast to classical measurements, QAE leverages the power of quantum computing to measure small probability events through amplitude amplification efficiently. Using QAE, we transcend the limitations of traditional measurement methods, which often ignore rare events by only sampling high probability events when computational resources limit the sample size. In the context of carbon market risk estimation, tail events can have significant consequences and the ability to capture and estimate these rare events is necessary. Different from the application of QAE in the field of chemistry, it is mainly to determine the ground state energy of molecules [39]. When applied to risk estimation, QAE is tasked with precisely measuring the probability distribution and computing the cumulative distribution function (CDF), rather than solely focusing on a single peak value or the optimal solution. In our paper, CDF refers to the sum of the probabilities that the loss rate is greater than the specified loss rate. However, existing QAE methods for estimating CDF need to traverse all probability distributions. This exhaustive traversal is essential to establish the full quantum space to pinpoint the regions of interest accurately. Such an approach demands many measurements, reducing the overall model efficiency.

To enhance efficiency in estimating the CDF, binary search is integrated with QAE. Binary search searches the target quantum state corresponding to a certain confidence level and determines the qubits of the target quantum state one by one. The space is divided into 2^n parts. Leveraging the characteristics of binary encoding, we pinpoint the quantum state starting from the highest

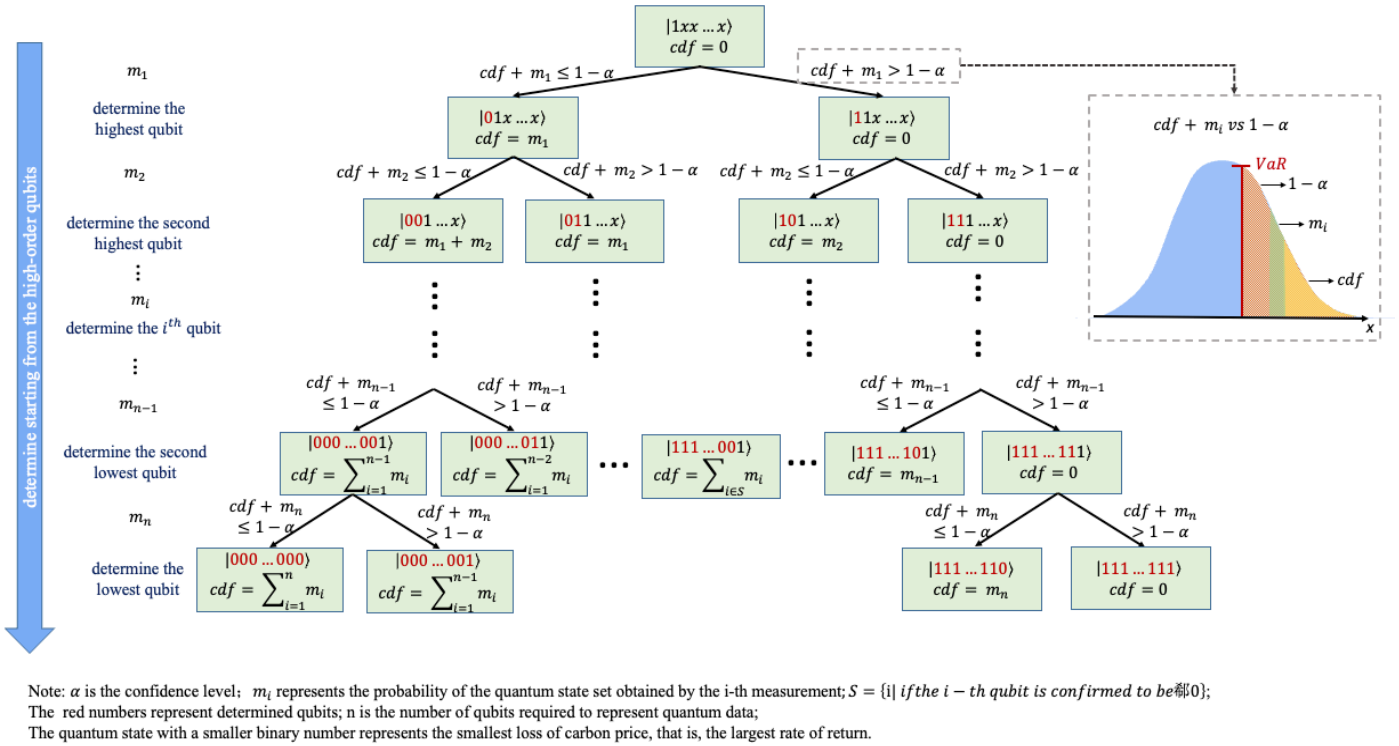

Note: α is the confidence level; m_i represents the probability of the quantum state set obtained by the i-th measurement; $S = \{i|\ if the\ i-th\ qubit\ is\ confirmed\ to\ be 都 0\}$;
The red numbers represent determined qubits; n is the number of qubits required to represent quantum data;
The quantum state with a smaller binary number represents the smallest loss of carbon price, that is, the largest rate of return.

Fig.4. Quantum amplitude estimation combined with binary search.

qubit, and each search shrinks the space size to which the target quantum state belongs by half and determines the qubit of the current bit. This allows us to locate the VaR result within no more than n iterations, where n is the number of qubits required to encode the quantum data.

Simultaneously, addressing the issue of encoding continuity becomes crucial. The continuity of quantum coding refers to the adjacency of the numerical ranges corresponding to the quantum state. The discontinuity of the encoding means the discontinuity and inaccuracy of the estimated CDF, which will in turn lead to the inaccuracy of the estimated VaR and CVaR. Confirming qubits starting from the highest bit ensures that all uncertain qubits appear in the lower bits, so that all sets of quantum states to be measured are continuous. For example, the first two digits of $|10x\rangle$ are determined, the quantum set to be measured is $|100\rangle\ and\ |101\rangle$. The numerical intervals corresponding to these quantum states are continuous. However, if we do not start from the highest bit, for example, if we try to locate the state $|1x1\rangle$, then the state $|101\rangle$ and $|111\rangle$ would be identified, leading to a discontinuity in the corresponding classical value since $|110\rangle$ is missing. This continuity lends rationality to the set of quantum states we target.

The details of QAE combined with binary search are as follows. The framework is shown in Fig. 6.

Initially in m1, use the binary search method to divide the quantum state space into two parts with the median of the quantum state as the boundary, one part is $|1x\dots x\rangle$ and the other part is $|0x\dots x\rangle$. Among them, what is measured is the space of quantum states greater than the median, that is, $|1x\dots x\rangle$. In other words, the median is the midpoint of the x-axis in the probability distribution diagram. This method is to determine the location of the "good" space relative to the median, so as to find the "good" space. Notably, with a binary search, our attention remains focused on the determined and next quantum position, while distant positions are ignored. For example, in a four-qubit system, having determined the first two positions as $|10\rangle$, we would mark $|101x\rangle$ (the final '1' arises due to binary search).

Subsequently, we measure and validate the quantum states. Comparing the measured probability m_i of the current set of quantum states determined by the binary search method with the sum of the previous cumulative probabilities cdf against a default confidence level α.cdf refers to the sum of probabilities greater than or equal to the current loss rate. If $(cdf + m_i)$ exceeds (1-α), which means that the "good" space is larger than the median, the current position is confirmed as $|1\rangle$; otherwise, means that the "good" space is smaller than the median, the current position is confirmed as $|0\rangle$. For positions determined as $|0\rangle$, we need to document the combined probability of the marked states, i.e., $cdf_{\text{new}} = cdf_{original} + m_i$. Through this method, the good space is determined and the size is reduced to half. Revisiting the previous example in the four-qubit system, the quantum state corresponding to VaR has determined that the first two qubits are $|10\rangle$. This means that in the first previous comparison, the initial cdf was 0, and the comparison found that the sum $(cdf + m_1)$ is the probability sum of $|1xxx\rangle$, i.e., m_1, was greater than 1-α, so the first qubit was confirmed to be $|1\rangle$, and not store m_1, so the $cdf_{new} = cdf = 0$. In the second comparison, since the cdf was still 0. The comparison found that the sum $(cdf + m_2)$ is the probability sum of $|11xx\rangle$, i.e., m_2, was smaller than 1-α, so the second qubit was confirmed to be $|0\rangle$, and stores m_2, so the $cdf_{new} = cdf + m_2 = m_2$, that is, the probability sum of $|1100\rangle$, $|1101\rangle$, $|1110\rangle$, and $|1111\rangle$.

Then the median is determined again based on the binary search method, and the above steps are repeated until all qubits of the quantum state are determined or the range is found. This method checks the aggregated probabilities of confirmed states ($cdf + m_i$) against (1-α), ensuring that by the iteration's end, we possess a state closest to the desired configuration, the quantum state corresponding to VaR. According to the quantum state corresponding to VaR, find the quantum state whose loss rate is greater than VaR, measure its probability, and finally calculate CVaR.

IV. Case Study

A. Settings

1) Data Sets

As the largest participant in the EU ETS, the European Climate Exchange (ECX) is an important indicator of the global carbon market. For this study, we use the daily carbon price from the EU ETS market to calculate the daily rate of returns, then take a negative number for the daily return to get the loss rate. The data comes from the European Energy Exchange and is expressed in euros per ton. Given the phased nature of the EU carbon market, we have chosen to focus on the third phase (2013-2020) of the market's development. Our dataset covers the period from January 1, 2015 to December 31, 2020, excluding public holidays. The data is split into two datasets without shuffling: training set (80%) and test set (20%), totaling 1544 data points. To enhance coding efficiency and accuracy, as well as to accelerate and stabilize data convergence, all historical loss rate processed from price data was min-max normalized into the range of [-1,1] and then evenly divided into 2^8 segments. Finally, we convert the numerical value of each segment into a binary format for processing in quantum computing.

2) VaR/CVaR Backtesting

The backtesting of VaR in the paper is the Kupiec Test. The test examines whether the number of times actual loss rates exceed the VaR estimates follows a binomial distribution with a success probability equal to the VaR confidence level. Let T be the total number of observations, N as the number of failures (i.e., the number of times the actual loss rate exceeds the predicted VaR), α as the given confidence level and p is the failure rate, that is, 1-α. Then the fail ratio and likelihood ratio (LR) [40] can be expressed as:

$$\text{fail ratio} = N/T \tag{7}$$

$$LR = 2ln\left(\frac{(1-N/T)^{T-N}(N/T)^{N}}{(1-p)^{T-N}(p)^{N}}\right) \tag{8}$$

The fail ratio can be directly compared with p. In order to conveniently express the difference, we introduce $\Delta\ \text{fail ratio} = |N/T - p|$. The smaller the value, the more accurate the estimation will be. And for LR, if LR surpasses the critical value (a chi-squared distribution with one degree of freedom) at a given significance level, the VaR model is rejected. Among them, the Kupiec test about LR is more basic and important. Only after passing the Kupiec test can the comparison of Δ fail ratio be meaningful.

The backtest of CVaR is Differences of Losses and CVaR (DLC) test. The DLC back test focuses on the difference between the actual loss rates that exceeded VaR and the CVaR values [41]. This statistic is defined as:

$$DLC = \left|\frac{1}{N}\sum_{i=1}^{N} X_i - \frac{1}{N}\sum_{i=1}^{N} CVaR_i\right| \tag{9}$$

where X_i is the actual loss rates that exceeded VaR. The smaller the DLC, the closer the expected value of CVaR is to the expected value of actual loss rates, and the higher the accuracy of CVaR measurement.

3) Quantum Computer Computational Time Cost

Our primary goal is to ascertain the real-world potential of quantum hardware in the context of risk assessment for carbon market returns. Therefore, it's crucial to evaluate the genuine computational time QAE would demand on a quantum processor, not just on classical computers [42].

We therefore consider both the time required to simulate the distribution using QCGAN's quantum generator and the subsequent measurements required for the QAE process. Each quantum process is associated with distinct circuit depths: $D_{QCGAN,i}$ for QCGAN and $D_{QAE,i}$ for QAE. The unified computing time considering a single execution of these two processes is calculated as follows:

$$T_i = T_P + T_G \times (D_{QCGAN,i} + D_{QAE,i}) + T_M \tag{9}$$

where T_P is the time to prepare the initial state, T_G is the average duration of a quantum gate, and T_M is the time needed to measure the qubits.

Extending to m distributions in the scenario requires simulation and measurement, with a cumulative computational time of:

$$T_{total} = \sum_{i=1}^{m} T_i \tag{10}$$

For this estimation, we will adopt the following time scales, which reflect aggressive yet realistic predictions for state-of-the-art quantum devices: $T_P + T_M = 1\mu s$, $T_G = 10ns$.

4) Hyperparameter and Implementation Details

TABLE I
Test Parameters

Parameter	Value	Parameter	Value
Input Dimension	3*1	Batch Size	32
Output Dimension	1	Learning Rate	0.001
Condition Qubits	3*8	Depth	2
Simulation Qubits	8	Hidden Dimension	2

The specific hyperparameters used for the various methods are detailed in Table I. For models involving neural networks, a batch size of 32, a learning rate of 0.001, a depth of 2, and a hidden dimension of 2 are employed. The input dimension is 3×1, signifying the historical loss rate from the past three days. Each daily loss rate is encoded by 8 qubits, culminating in 3×8 qubits for the condition. Meanwhile, the output dimension is 1, representing the simulated future daily rate of return, which is also depicted by 8 qubits, thus totaling 8 qubits for the simulation. Given that a binary code of 8 qubits represents each daily loss rate, the total number of coded segments amounts to 2^8.

B. Accuracy Comparison of Optimal Result

We compare the proposed QCGAN-QAE with the existing QCGAN and CGAN models to validate its effectiveness. The

TABLE II
COMPARISON OF ACCURACY BETWEEN CGAN, QCGAN AND QCGAN-QAE.

	Model	CGAN			QCGAN			QCGAN-QAE		
	Confidence level	90%	95%	99%	90%	95%	99%	90%	95%	99%
VaR	N (fail num.)	34	20	**3**	54	48	35	**28**	**18**	3
	fail ratio (%)	11.00%	6.47%	**0.97%**	17.48%	15.53%	11.33%	**9.06%**	**5.83%**	0.97%
	Δ fail ratio (%)	1.00%	1.47%	**0.03%**	7.48%	10.53%	10.33%	**0.94%**	**0.83%**	0.03%
	LR	0.3358	1.2958	**0.0027**	16.0628	47.4754	109.5332	**0.3112**	**0.4217**	0.0027
CVaR	Loss mean (fail.)	5.1126	4.8289	**11.8597**	4.1407	4.3693	4.9903	**5.4800**	**6.4599**	9.2344
	CVaR mean (fail.)	3.3847	7.4496	**9.9498**	2.4542	2.6459	3.0369	**3.9583**	**6.1182**	16.0058
	DLC	1.7279	2.6208	**1.9099**	1.6866	1.7234	1.9534	**1.5217**	**0.3417**	6.7714

comparison is based on their ability to accurately estimate the VaR and CVaR of the carbon market.

Table. II shows the comparison of accuracy between CGAN, QCGAN and QCGAN-QAE. We found that the LR value of the original QCGAN is too large and exceeds the critical value, so it failed to pass the Kupiec test at all three confidence levels. Therefore, the estimation ability of QCGAN could not reflect the real VaR and CVaR situations, and we only analyzed CGAN and QCGAN-QAE that passed the Kupiec test in the following. The table shows that at 90% and 95% confidence levels, QCGAN-QAE performs better than CGAN in both VaR and CVaR prediction accuracy. Specifically, at 90% confidence level, in terms of Δ fail ratio, QCGAN-QAE decreased by 6.00%; in terms of DLC, QCGAN-QAE decreased by 11.93%. At 95% confidence level, in terms of Δ fail ratio, QCGAN-QAE decreased by 43.54%; in terms of DLC, QCGAN-QAE decreased by 86.96%. However, at the 99% confidence level, QCGAN-QAE and CGAN have the same estimation performance for VaR, while at the estimation level of CVaR, the classic CGAN is 254.54% better than QCGAN-QAE.

The poor prediction accuracy of QCGAN may be attributed to several key reasons. First, the existing QCGAN requires a more complex quantum circuit design, and the sequence of conditional data interaction and data simulation hinders effective quantum information exchange. Second, the method relies only on direct measurements, it is easy to produce errors when measuring low-probability extreme values. The data in the table also verify this phenomenon; while QCGAN shows relatively strong performance at the 90% confidence level, its prediction performance drops sharply at the 99% confidence level.

As for why QCGAN-QAE performs worse than classical CGAN at the 99% confidence level may be due to the limitation of qubits. In our proposed QCGAN-QAE model, the number of qubits used is directly related to the accuracy of the prediction, so there may still be some limitations in the accuracy of extreme values, resulting in a 99% confidence level CVaR estimation error. As quantum computers develop and more and more qubits become available, this limitation will progressively diminish.

In general, this comparison shows that QCGAN-QAE has improved accuracy in most cases compared with traditional CGAN and QCGAN estimation results, illustrating the huge potential of quantum algorithms in carbon market risk estimation.

C. Computational Efficiency Comparison of Optimal Result

To compare the advantages of the quantum algorithm QCGAN-QAE in terms of computational efficiency, we compared the running time and the epochs required for convergence of our proposed QCGAN-QAE with the traditional CGAN, which is similar to the accuracy.

TABLE III
COMPARISON OF COMPUTATIONAL EFFICIENCY BETWEEN CGAN AND QCGAN-QAE.

	CGAN			QCGAN-QAE		
	90%	95%	99%	90%	95%	99%
Quantum computer (s)	/	/	/	**0.0020**	**0.0020**	**0.0021**
Traditional computer (s)	169	168	167	**992**	**990**	**994**
Epoch	300	300	300	**30**	**30**	**30**

Table. III shows the results of various time indicators required to execute each model of carbon market risk estimation. For running time, we compare the running time of quantum algorithms on quantum computing with the running time of traditional algorithms on traditional computers. Especially when the confidence level is 90% and 95%, QCGAN-QAE is slightly better than CGAN in accuracy, and the required running time is only 1/84500 (a reduction of 99.9988%) and 1/84000 of CGAN (a reduction of 99.9988%). Even when the confidence level is 99%, QCGAN-QAE has a huge advantage when the accuracy is slightly worse than CGAN, and the required running time is only 1/79524 of CGAN (a reduction of 99.9987%). Therefore, comparing the running time of classical algorithms on classical computers and the running time of quantum algorithms on quantum computers, quantum algorithms have strong advantages. For the epochs required for convergence, QCGAN-QAE requires only 30 epochs to achieve convergence, compared to the 300 epochs needed by CGAN, the required epochs are reduced by 90%, which means that the quantum algorithm has the advantage of convergence.

The computational efficiency of QCGAN-QAE exceeds that of CGAN, which may due to quantum parallelism and a more favorable optimization environment. Quantum parallelism allows QCGAN to perform multiple computations simultaneously, speeding up efficiency, whereas CGAN on classical computers can only perform operations sequentially. Furthermore, quantum computers can more effectively navigate complex, potentially non-convex GAN optimization environments, enabling QCGAN to find more favorable convergence paths. Therefore, the outstanding computational speed of QCGAN-QAE from its ability to perform multiple computations simultaneously and traverse complex optimization environments more efficiently.

In general, this comparison demonstrates the strong advantages of our proposed QCGAN-QAE algorithm in terms of

TABLE IV
COMPARISON OF ACCURACY BETWEEN QCGANS WITH DIFFERENT QUANTUM CIRCUIT STRUCTURES.

	Model	QCGAN(original)			QCGAN(modified)			QCGAN(modified+QFC)		
	Confidence level	90%	95%	99%	90%	95%	99%	90%	95%	99%
VaR	N (fail num.)	54	48	35	44	19	**4**	**42**	**17**	4
	fail ratio (%)	17.48%	15.53%	11.33%	14.24%	6.15%	**1.29%**	**13.59%**	**5.50%**	1.29%
	Δ fail ratio	7.48%	10.53%	10.33%	4.24%	1.15%	**0.29%**	**3.59%**	**0.50%**	0.29%
	LR	16.0628	47.4754	109.5332	5.5291	0.8026	**0.2477**	**4.0298**	**0.1587**	0.2477
CVaR	Loss mean (fail.)	4.1407	4.3693	4.9903	4.5261	6.6463	**10.6796**	**4.6087**	**6.7394**	10.3159
	CVaR mean (fail.)	2.4542	2.6459	3.0369	3.1831	7.4391	**27.1200**	**3.6205**	**7.1417**	35.2923
	DLC	1.6866	1.7234	1.9534	1.3430	0.7927	**16.4404**	**0.9882**	**0.4023**	24.9763

computational efficiency when the accuracy is roughly equivalent to or better than the traditional algorithm.

D. Accuracy Comparison of QCGANs with Different Quantum Circuit Structures

This experiment aims to evaluate the performance of the proposed QCGAN algorithm, in particular, to compare different quantum circuit structures and their accuracy in estimating carbon market risk. This is crucial to understand how different circuit architectures affect the results and to choose the most suitable structure for practical applications. The considered structures include original, proposed, and proposed quantum circuits with additional QFC.

Table. IV shows the accuracy comparison of QCGANs with different quantum circuit structures. The results show that the estimation accuracy of the modified QCGAN is significantly better than that of the original QCGAN. Since the LR value of the original QCGAN is too large and exceeds the critical value, so it could not pass the Kupiec test at 90%, 95% and 99% confidence levels, but the modified model can pass the 95% and 99% confidence level tests. This performance suggests that quantum circuits that perform entanglement followed by rotation can better capture the distribution of loss rate. In addition, we compare the estimation accuracy of the model with or without adding QFC. It is found that at 90% and 95% confidence levels, those with QFC perform better on both VaR and CVaR. Specifically, at 90% confidence level, in terms of Δ fail ratio, QCGAN-QAE decreased by 15.33%; in terms of DLC, QCGAN-QAE decreased by 26.42%. At 95% confidence level, in terms of Δ fail ratio, QCGAN-QAE decreased by 56.52%; in terms of DLC, QCGAN-QAE decreased by 49.25%. And at 99% confidence level, although the effects of both VaR are the same, QCGAN without QFC the DLC is relatively small. However, it should be noted that even though the DLC without QFC (16.4404) is still too large, the comparison between the two is not meaningful, and we will solve this problem in the next Sec. IV.E. In summary, QCGAN with QFC is still slightly better.

The experimental results validated the rationale behind swapping the entanglement and rotation stage. The enhancement in accuracy brought by the swap might stem from the strong quantum correlations established through entanglement prior to the rotation stage, which provides a more favorable condition for the rotation operations. Consequently, this improves the quantum circuit's expressiveness and efficiency, further elevating the accuracy of the estimation. In addition, the advantage of adding QFC is its ability to interact between information more effectively so that the information can be fully characterized and ultimately improve the estimation accuracy.

In conclusion, the experiments show that modifying the quantum circuit structure and adding QFC can significantly enhance the performance of the QCGAN-QAE algorithm in terms of carbon market risk estimation. This improvement is critical to developing more accurate and efficient carbon market risk management tools.

E. Comparison of QAE and Measure

This experiment aims to demonstrate the advantages of QAE over classical measurement methods and highlight the improved time efficiency of combining QAE with binary search methods. In this section, we compare the performance of QAE with direct classical measurement methods in estimating the amplitudes of quantum states generated by QCGAN models. Furthermore, we also evaluate the computational efficiency obtained by integrating the binary search method into QAE instead of using QAE alone.

Table. V shows the estimated performance of QCGAN with or without QAE. The results show that after adding QAE, the estimation accuracy is improved. When the confidence level is

TABLE V
COMPARE THE RESULTS OF QCGAN COMBINED WITH QAE ON ESTIMATION ACCURACY.

	Model	QCGAN			QCGAN-QAE		
	Confidence level	90%	95%	99%	90%	95%	99%
VaR	N (fail num.)	42	**17**	4	**28**	18	**3**
	fail ratio (%)	13.59%	**5.50%**	1.29%	**9.06%**	5.83%	**0.97%**
	Δ fail ratio	3.59%	**0.50%**	0.29%	**0.94%**	0.83%	**0.03%**
	LR	4.0298	**0.1587**	0.2477	**0.3112**	0.4217	**0.0027**
CVaR	Loss mean (fail.)	4.6087	6.7394	10.3159	**5.4800**	**6.4599**	**9.2344**
	CVaR mean (fail.)	3.6205	7.1417	35.2923	**3.9583**	**6.1182**	**16.0058**
	DLC	0.9882	0.4023	24.9763	**1.5217**	**0.3417**	**6.7714**

90%, the LR of QCGAN without QAE is too large to pass the Kupiec test, while the QCGAN with QAE passes the test. When the confidence level is 95%, we found that although the performance of QCGAN with QAE in the Δ fail ratio has declined, it still passed the test successfully, and the performance of QCGAN-QAE in DLC has improved by 15.06%. The most important thing is the performance improvement at 99% confidence level. In terms of Δ fail ratio, QCGAN-QAE has been reduced by 89.66%, and in terms of DLC, it has been reduced by 72.89%. This also solves the previously mentioned problem that DLC has always been too large.

The reason why QAE can improve the prediction accuracy and solve the CVaR prediction problem under 99% confidence may be the nature of the QAE algorithm itself. QAE is a vital quantum algorithm for estimating the amplitude of quantum states, which is crucial for various quantum computing applications. QAE improves the accuracy of predictions by amplifying the amplitude of a given quantum state. This property has important implications for measuring quantum states with tiny probabilities, that is, the probability of extreme loss rates occurring in our case. In contrast, direct measurement is a simple technique but often requires multiple repetitions to obtain precise results.

TABLE VI
COMPARISON OF COMPUTATIONAL TIME COMBINED WITH BINARY SEARCH.

Model	Confidence level	Quantum computer (s)
QCGAN-QAE	90%	0.0122
	95%	0.0064
	99%	0.0017
QCGAN-QAE (binary search)	90%	**0.0020**
	95%	**0.0020**
	99%	**0.0021**

Table. VI shows the comparison of computational time combined with binary search. By comparing the results, we can find that at the 90% confidence level, the QAE efficiency combined with the bisection method reduces the running time on the quantum computer by 83.61%; at the 95% confidence level, the running time is shortened by 68.75%. As for the 99% confidence level, the running time increased by 23.53%. In general, when the confidence is small, the acceleration combined with the binary search method is more obvious. When the confidence level is particularly large, the QAE may only be as good as that with the binary search method.

The efficiency improvement of QAE comes from binary search. Binary search is a very classic algorithm. Combining the binary search method with QAE speeds up the computation process by reducing the number of operations required. The time complexity of QAE combined with the binary search method is reduced from O(N) to O(logN). As for the 99% confidence level, it takes longer to combine binary search because the original QAE is measured from the quantum state that represents the largest loss rate, and the VaR with a 99% confidence level is generally a large loss rate so fewer measurements may be required.

In conclusion, experiments demonstrate that integrating binary search and QAE can dramatically speed up the computation process. This improvement has important implications for quantum computing applications, especially in risk estimation.

F. Parameter Sensitivity Analysis

Typically, the performance of a robust QCGAN-QAE should be relatively high when the depth fluctuates within a reasonable range. To demonstrate the universality of QCGAN-QAE's predictions, we compared QCGAN-QAE models with depths of 2, 4, and 6.

Table. VII shows that within the selected depth range, the model's performance is not sensitive to the depth choice. This insensitivity might be attributed to our modified QCGAN and replacing the simple measure with QAE. Specifically, the refined QCGAN ensures that the quantum circuit's essential properties do not change significantly with depth. Moreover, using QAE helps obtain more accurate estimates, irrespective of the circuit depth.

Additionally, it is important to note that while increasing the depth of a quantum circuit can sometimes lead to more expressive models, it also increases the risk of overfitting and the impact of noise. The chosen range of depths seems optimal for balancing the trade-off between model efficiency and accuracy.

VI. CONCLUSION

Carbon market risk estimation plays an important role in global environmental governance and corporate strategic decision-making. To meet the carbon market's demand for higher accuracy and efficiency in risk estimation, we introduce the QCGAN-QAE framework. This framework combines the estimation accuracy of QCGAN with the computational efficiency of QAE, forming in a novel quantum computing-based carbon market risk estimation framework. Specifically,

TABLE VII
RESULTS OF VAR/CVAR ESTIMATED BY QCGAN-QAE WITH DIFFERENT DEPTHS.

	Model	2			4			6		
	Confidence level	90%	95%	99%	90%	95%	99%	90%	95%	99%
VaR	N (fail num.)	**28**	**18**	**3**	25	18	2	34	19	2
	fail ratio (%)	**9.06%**	**5.83%**	**0.97%**	8.09%	5.83%	0.65%	11.00%	6.15%	0.65%
	Δ fail ratio (%)	**0.94%**	**0.83%**	**0.03%**	1.91%	0.83%	0.35%	1.00%	1.15%	0.35%
	LR	**0.3112**	**0.4217**	**0.0027**	1.3303	0.4217	0.4438	0.3358	0.8026	0.4438
CVaR	Loss mean (fail.)	5.4800	6.4599	9.2344	5.7935	6.4597	13.9113	**4.6143**	**5.2242**	**13.9113**
	CVaR mean (fail.)	3.9583	6.1182	16.0058	4.3859	5.3343	25.2832	**3.6005**	**5.4312**	**9.9307**
	DLC	1.5217	0.3417	6.7714	1.4076	1.1254	11.3720	**1.0137**	**0.2070**	**3.9806**

by optimizing the circuit structure of QCGAN, we have further enhanced the accuracy of VaR and CVaR estimation. Moreover, the QAE, integrated with the binary search method and leveraging its capability to amplify quantum amplitudes, not only improves risk estimation accuracy with limited measurements but also greatly improves model efficiency. Empirical evidence demonstrates that the QCGAN-QAE framework improves the estimation accuracy compared to both the classical CGAN and the original QCGAN. Although our primary focus is on carbon market risks, the QCGAN-QAE framework also heralds new possibilities for risk estimation in other domains. In future research works, aiming to reduce reliance on the number of quantum bits, we intend to employ angular rotation encoding to refine our quantum encoding approach. Additionally, our focus will pivot towards devising strategies for more effectively selecting and adjusting QCGAN-QAE algorithm parameters to enhance its performance further.

REFERENCES

[1] W. J. Ripple, C. Wolf, T. M. Newsome, P. Barnard, W. R. Moomaw, and P. Grandcolas, "World Scientists' Warning of a Climate Emergency," *Bioscience*, 2019, doi: 10.1093/biosci/biz088/5610806.

[2] G. Daskalakis, "Are the European Carbon Markets Efficient?," in *Are the European Carbon Markets Efficient?: Daskalakis, George*, [S.l.] : SSRN, 2014. Accessed: Sep. 10, 2023. [Online]. Available: http://www.zbw.eu/econis-archiv/handle/11159/18311

[3] S. M. Idrees, M. A. Alam, and P. Agarwal, "A Prediction Approach for Stock Market Volatility Based on Time Series Data," *IEEE Access*, vol. 7, pp. 17287–17298, 2019, doi: 10.1109/ACCESS.2019.2895252.

[4] C. Dritsaki, "The performance of hybrid ARIMA-GARCH modeling and forecasting oil price," vol. 8, no. 3, 2018.

[5] A. Rutkowska-Ziarko, L. Markowski, C. Pyke, and S. Amin, "Conventional and downside CAPM: The case of London stock exchange," *Glob. Finance J.*, vol. 54, p. 100759, Nov. 2022, doi: 10.1016/j.gfj.2022.100759.

[6] P. Le, K. Kim, and Y. Su, "Reexamination of Estimating Beta Coefficient as a Risk Measure in CAPM," *J. Asian Finance Econ. Bus.*, vol. 5, pp. 11–16, Feb. 2018, doi: 10.13106/jafeb.2018.vol5.no1.11.

[7] J. Freyberger, A. Neuhierl, and M. Weber, "Dissecting Characteristics Nonparametrically," *Rev. Financ. Stud.*, vol. 33, no. 5, pp. 2326–2377, May 2020, doi: 10.1093/rfs/hhz123.

[8] C. Wegener and T. Basse, "The Stability of Factor Sensitivities of German Stock Market Sector Indices: Empirical Evidence and Some Thoughts about Practical Implications," *J. Risk Financ. Manag.*, vol. 12, no. 3, Art. no. 3, Sep. 2019, doi: 10.3390/jrfm12030140.

[9] L. J. Hong, Z. Hu, and G. Liu, "Monte Carlo Methods for Value-at-Risk and Conditional Value-at-Risk: A Review," *ACM Trans. Model. Comput. Simul.*, vol. 24, no. 4, p. 22:1-22:37, Nov. 2014, doi: 10.1145/2661631.

[10] Z. He, "Sensitivity estimation of conditional value at risk using randomized quasi-Monte Carlo," *Eur. J. Oper. Res.*, vol. 298, no. 1, pp. 229–242, Apr. 2022, doi: 10.1016/j.ejor.2021.11.013.

[11] B. Zhu, L. Huang, L. Yuan, S. Ye, and P. Wang, "Exploring the risk spillover effects between carbon market and electricity market: A bidimensional empirical mode decomposition based conditional value at risk approach," *Int. Rev. Econ. Finance*, vol. 67, pp. 163–175, May 2020, doi: 10.1016/j.iref.2020.01.003.

[12] B. Zhu, X. Zhou, X. Liu, H. Wang, K. He, and P. Wang, "Exploring the risk spillover effects among China's pilot carbon markets: A regular vine copula-CoES approach," *J. Clean. Prod.*, vol. 242, p. 118455, Jan. 2020, doi: 10.1016/j.jclepro.2019.118455.

[13] Z.-H. Feng, Y.-M. Wei, and K. Wang, "Estimating risk for the carbon market via extreme value theory: An empirical analysis of the EU ETS," *Appl. Energy*, vol. 99, pp. 97–108, Nov. 2012, doi: 10.1016/j.apenergy.2012.01.070.

[14] D. Grinko, J. Gacon, C. Zoufal, and S. Woerner, "Iterative quantum amplitude estimation," *Npj Quantum Inf.*, vol. 7, no. 1, Art. no. 1, Mar. 2021, doi: 10.1038/s41534-021-00379-1.

[15] Y. Suzuki, S. Uno, R. Raymond, T. Tanaka, T. Onodera, and N. Yamamoto, "Amplitude estimation without phase estimation," *Quantum Inf. Process.*, vol. 19, no. 2, p. 75, Jan. 2020, doi: 10.1007/s11128-019-2565-2.

[16] D. J. Egger, R. García Gutiérrez, J. C. Mestre, and S. Woerner, "Credit Risk Analysis Using Quantum Computers," *IEEE Trans. Comput.*, vol. 70, no. 12, pp. 2136–2145, Dec. 2021, doi: 10.1109/TC.2020.3038063.

[17] S. Woerner and D. J. Egger, "Quantum risk analysis," *Npj Quantum Inf.*, vol. 5, no. 1, Art. no. 1, Feb. 2019, doi: 10.1038/s41534-019-0130-6.

[18] L. Xu, "Synthesizing Tabular Data using Conditional GAN".

[19] J. Moon, S. Jung, S. Park, and E. Hwang, "Conditional Tabular GAN-Based Two-Stage Data Generation Scheme for Short-Term Load Forecasting," *IEEE Access*, vol. 8, pp. 205327–205339, 2020, doi: 10.1109/ACCESS.2020.3037063.

[20] W. Liu, Y. Zhang, Z. Deng, J. Zhao, and L. Tong, "A hybrid quantum-classical conditional generative adversarial network algorithm for human-centered paradigm in cloud," *EURASIP J. Wirel. Commun. Netw.*, vol. 2021, no. 1, p. 37, Feb. 2021, doi: 10.1186/s13638-021-01898-3.

[21] G. Liu *et al.*, "Super-resolution perception for wind power forecasting by enhancing historical data," *Front. Energy Res.*, vol. 10, 2022, Accessed: Oct. 16, 2023. [Online]. Available: https://www.frontiersin.org/articles/10.3389/fenrg.2022.959333

[22] Y. Cao, H. Zhao, G. Liang, J. Zhao, H. Liao, and C. Yang, "Fast and explainable warm-start point learning for AC Optimal Power Flow using decision tree," *Int. J. Electr. Power Energy Syst.*, vol. 153, p. 109369, Nov. 2023, doi: 10.1016/j.ijepes.2023.109369.

[23] A. Steane, "Quantum computing," *Rep. Prog. Phys.*, vol. 61, no. 2, p. 117, Feb. 1998, doi: 10.1088/0034-4885/61/2/002.

[24] L. Gyongyosi and S. Imre, "A Survey on quantum computing technology," *Comput. Sci. Rev.*, vol. 31, pp. 51–71, Feb. 2019, doi: 10.1016/j.cosrev.2018.11.002.

[25] A. Creswell, T. White, V. Dumoulin, K. Arulkumaran, B. Sengupta, and A. A. Bharath, "Generative Adversarial Networks: An Overview," *IEEE Signal Process. Mag.*, vol. 35, no. 1, pp. 53–65, Jan. 2018, doi: 10.1109/MSP.2017.2765202.

[26] M. Mirza and S. Osindero, "Conditional Generative Adversarial Nets." arXiv, Nov. 06, 2014. doi: 10.48550/arXiv.1411.1784.

[27] E. G. Brown, O. Goktas, and W. K. Tham, "Quantum Amplitude Estimation in the Presence of Noise." arXiv, Jun. 24, 2020. Accessed: Sep. 20, 2023. [Online]. Available: http://arxiv.org/abs/2006.14145

[28] G. Brassard, P. Hoyer, M. Mosca, and A. Tapp, "Quantum Amplitude Amplification and Estimation," vol. 305, 2002, pp. 53–74. doi: 10.1090/conm/305/05215.

[29] H. Kwon and J. Bae, "A Hybrid Quantum-Classical Approach to Mitigating Measurement Errors in Quantum Algorithms," *IEEE Trans. Comput.*, vol. 70, no. 9, pp. 1401–1411, Sep. 2021, doi: 10.1109/TC.2020.3009664.

[30] J. W. Taylor, "Forecasting Value at Risk and Expected Shortfall Using a Semiparametric Approach Based on the Asymmetric Laplace Distribution," *J. Bus. Econ. Stat.*, vol. 37, no. 1, pp. 121–133, Jan. 2019, doi: 10.1080/07350015.2017.1281815.

[31] N. Liu, C. Liu, B. Da, T. Zhang, and F. Guan, "Dependence and risk spillovers between green bonds and clean energy markets," *J. Clean. Prod.*, vol. 279, p. 123595, Jan. 2021, doi: 10.1016/j.jclepro.2020.123595.

[32] H.-L. Huang *et al.*, "Experimental Quantum Generative Adversarial Networks for Image Generation," *Phys. Rev. Appl.*, vol. 16, no. 2, p. 024051, Aug. 2021, doi: 10.1103/PhysRevApplied.16.024051.

[33] N.-R. Zhou, T.-F. Zhang, X.-W. Xie, and J.-Y. Wu, "Hybrid quantum–classical generative adversarial networks for image generation via learning discrete distribution," *Signal Process. Image Commun.*, vol. 110, p. 116891, Jan. 2023, doi: 10.1016/j.image.2022.116891.

[34] S. Y.-C. Chen, S. Yoo, and Y.-L. L. Fang, "Quantum Long Short-Term Memory," in *ICASSP 2022 - 2022 IEEE International Conference on Acoustics, Speech and Signal Processing (ICASSP)*, Singapore, Singapore: IEEE, May 2022, pp. 8622–8626. doi: 10.1109/ICASSP43922.2022.9747369.

[35] S. Sim, P. D. Johnson, and A. Aspuru-Guzik, "Expressibility and Entangling Capability of Parameterized Quantum Circuits for Hybrid Quantum-Classical Algorithms," *Adv. Quantum Technol.*, vol. 2, no. 12, p. 1900070, 2019, doi: 10.1002/qute.201900070.

[36] D. Zhu *et al.*, "Training of quantum circuits on a hybrid quantum computer," *Sci. Adv.*, vol. 5, no. 10, p. eaaw9918, Oct. 2019, doi: 10.1126/sciadv.aaw9918.

[37] Y. Cao, X. Zhou, X. Fei, H. Zhao, W. Liu, and J. Zhao, "Linear-layer-enhanced quantum long short-term memory for carbon price

forecasting," *Quantum Mach. Intell.*, vol. 5, no. 2, p. 26, Jul. 2023, doi: 10.1007/s42484-023-00115-2.
[38] Y. Lu, V. Roychowdhury, and L. Vandenberghe, "Distributed Parallel Support Vector Machines in Strongly Connected Networks," *IEEE Trans. Neural Netw.*, vol. 19, no. 7, pp. 1167–1178, Jul. 2008, doi: 10.1109/TNN.2007.2000061.
[39] T. E. O'Brien *et al.*, "Calculating energy derivatives for quantum chemistry on a quantum computer," *Npj Quantum Inf.*, vol. 5, no. 1, Art. no. 1, Dec. 2019, doi: 10.1038/s41534-019-0213-4.
[40] M. Orhan and B. Köksal, "A comparison of GARCH models for VaR estimation," *Expert Syst. Appl.*, vol. 39, no. 3, pp. 3582–3592, Feb. 2012, doi: 10.1016/j.eswa.2011.09.048.
[41] J. Yang, G. Tang, D. Yang, and J. Zhang, "Risk Measurement and Performance Evaluation of Equity Funds Based on ARMA-GARCH Family Model," *Open J. Stat.*, vol. 10, no. 02, Art. no. 02, Apr. 2020, doi: 10.4236/ojs.2020.102022.
[42] G. G. Guerreschi and A. Y. Matsuura, "QAOA for Max-Cut requires hundreds of qubits for quantum speed-up," *Sci. Rep.*, vol. 9, no. 1, Art. no. 1, May 2019, doi: 10.1038/s41598-019-43176-9.